ELSEVIER

Journal of Alloys and Compounds 404–406 (2005) 669–674

Journal of ALLOYS AND COMPOUNDS

www.elsevier.com/locate/jallcom

Effects of Cr on the structural and electrochemical properties of TiV-based two-phase hydrogen storage alloys

Hongge Pan*, Rui Li, Mingxia Gao, Yongfeng Liu, Qidong Wang

Department of Materials Science and Engineering, Zhejiang University, Hangzhou 310027, PR China

Received 8 June 2004; received in revised form 31 December 2004
Available online 15 July 2005

Abstract

TiV-based two-phase hydrogen storage alloys are promising candidates for negative electrode materials of Ni/MH batteries. In this work, phase structures and electrochemical properties of the $Ti_{0.8}Zr_{0.2}V_{2.7}Mn_{0.5}Cr_xNi_{1.75}$ ($x = 0 \sim 0.7$) alloys were systematically investigated to get an overall evaluation of Cr in the TiV-based alloys. It was found by XRD and Rietveld analysis that all the alloys consisted of a C14 Laves phase with hexagonal structure and a V-based solid solution phase with BCC structure. With the increasing Cr contents, the abundance of V-based phase increased while the C14 Laves phase decreased gradually. Electrochemical investigations indicated that besides the anticipated improvement of cyclic life, the increasing Cr content also lead to a better high rate dischargeability (HRD) in a certain range, but the discharge capacity decreased with excessive Cr content, which can be attributed to the variation of the composition, abundance and distribution of the two phases in the alloys. Electrochemical impedance spectroscopy (EIS), linear polarization, anode polarization and potentiostatic discharge were employed to study the kinetic properties and the results indicated that HRD of the alloy electrodes were controlled mainly with the hydrogen diffusion resistance inside the alloy particles.

Keywords: Hydrogen storage materials; Metal hydrides; Phase structure; Electrochemical property

1. Introduction

TiV-based two-phase hydrogen storage alloys are promising candidates for negative electrode materials of Ni/MH batteries [1–5]. These alloys are developed from Ti-based Laves phase alloys. Zhu et al. [6–8] improved the overall performance of the Ti-based Laves phase alloys by element substitution and super-stoichiometry and get the TiV-based two-phase alloys. 'Two-phase' refers to a C14 Laves phase and a V-based solid solution phase. The V-based solid solution phase is the major hydrogen-absorbing phase, while the C14 Laves phase is not only a hydrogen-absorbing phase, but also proved to be a catalyst for the electrochemical hydrogenation and dehydrogenation process of the V-based phase [5]. The cooperation of the two phases gives the alloy a favorable electrochemical performance, especially the discharge capacity. However, as a developing alloy series, the Ti–V-based alloys still have many obstacles to overcome on the way to commercialization, such as the relatively dissatisfactory cycle life and high rate dischargeability of the alloys.

Composition optimization is commonly an effective way to improve the performance of hydrogen storage alloys. Yu et al. [9] reported that Cr substitution for Mn in the Ti-based AB_2 type alloy electrode effectively improved the cycle life of the electrode by reducing the dissolution of V in alkali solution and restraining the formation of TiO_2 film, which was believed to be the dominating factor in the degradation of the alloy [10]. Kim et al. [11] reported that Cr substitution for V in the V–Ti alloy improved the cycle life markedly, but the discharge capacity decreased rapidly with increasing Cr content.

Considering the negative effect of Cr on the capacity and positive effect on the cyclic stability of hydrogen storage alloys, it is important to investigate the role of Cr in the TiV-based two-phase alloys. In this work, Cr content in the TiV-

* Corresponding author. Tel.: +86 571 8795 2576; fax: +86 571 8795 1152.
E-mail address: honggepan@zju.edu.cn (H. Pan).

0925-8388/$ – see front matter © 2005 Elsevier B.V. All rights reserved.
doi:10.1016/j.jallcom.2005.05.005

based alloys was separately tuned to get an overall evaluation of Cr in the TiV-based alloys and optimize the composition of the alloys accordingly. The phase composition, microstructure, electrochemical properties of the alloys and their correlations are discussed.

2. Experimental

The $Ti_{0.8}Zr_{0.2}V_{2.7}Mn_{0.5}Cr_xNi_{1.75}$ ($x = 0 \sim 0.7$) alloys were prepared by induction levitation melting of the constituent metals in a water-cooled copper crucible under argon atmosphere. The ingots were turned over and remelted twice for homogeneity. Part of the alloys were mechanically crushed and ground into powders with a dimension of 300-mesh for XRD and electrochemical measurements.

Crystal structures and lattice parameters of the alloys were determined by X-ray powder diffraction (XRD) using Cu Kα radiation. The XRD patterns were analyzed by the Rietveld Method [12]. Microstructures were examined on polished cross sections of the ingots by a scanning electron microscope with an energy dispersive X-ray spectroscopy (SEM/EDX).

All test electrodes were prepared by mixing 0.1g alloy powder with 0.4 g carbonyl nickel powder and then cold-pressing the mixture under a pressure of 25 MPa into a pellet with the diameter of 10 mm and thickness of about 1 mm. The electrochemical measurements were performed in a half-cell consisting of a working electrode (MH electrode), a sintered $Ni(OH)_2$/NiOOH counter electrode and a Hg/HgO reference electrode. The electrolyte was a 6 M KOH solution, controlled at $30 \pm 1^{\circ}$. The discharge capacity of the electrode was determined by the galvanostatic method. Each electrode was charged at 100 mA/g for 5 h followed by 10 min rest and then discharged at 60 mA/g to the cut-off potential of –0.6 V versus the Hg/HgO reference electrode. Electrochemical impedance spectroscopy (EIS) measurements were conducted at 50% depth of discharge (DOD) using Solartron SI1287 Electrochemical Interface with a 1255B Frequency Response Analyzer, using the ZPLOT electrochemical impedance software. Before EIS measurements, the test electrodes were completely activated. The EIS of the electrodes were obtained in the frequency range of 100 kHz–5 mHz with an ac amplitude of 5 mV under open-circuit conditions. The linear polarization curves and the anode polarization curves of the test electrodes were measured by scanning the electrode potentials (Solartron SI1287 potentiostat, using the CorrWare electrochemistry/corrosion software) at the rate of 0.1 mV/s from –5 to 5 mV (versus open-circuit potential) and 5 mV/s from 0 to 1200 mV (versus open-circuit potential) at 50% depth of discharge (DOD), respectively. For the potentiostatic discharge, the test electrodes in fully charged state were discharged at +600 mV potential step for 3600 s on Solartron SI1287 potentiostat, using the CorrWare electrochemistry/corrosion software.

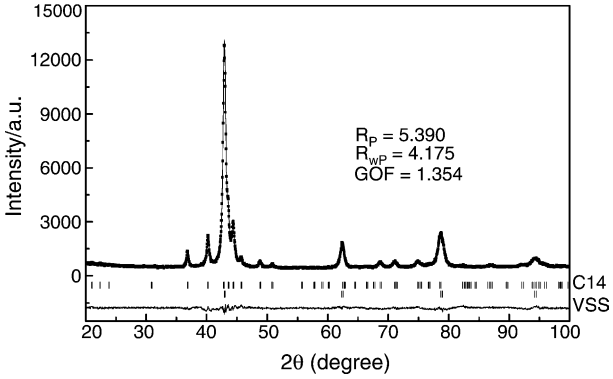

Fig. 1. The XRD/Rietveld analysis pattern of the $Ti_{0.8}Zr_{0.2}V_{2.7}Mn_{0.5}Cr_{0.1}Ni_{1.75}$ hydrogen storage alloy.

3. Results and discussion

Fig. 1 shows the XRD/Rietveld analysis pattern of the $Ti_{0.8}Zr_{0.2}V_{2.7}Mn_{0.5}Cr_{0.1}Ni_{1.75}$ alloy. The cell parameters and phase abundance of all the alloys figured out by the XRD/Rietveld analysis are listed in Table 1. All the alloys are composed of a C14 Laves phase with hexagonal structure and a V-based solid solution phase with bcc structure. With the increasing Cr contents, the abundance of V-based phase increased from 53.8 wt.% ($x = 0$) to 77.8 wt.% ($x = 0.7$) while the C14 Laves phase decreased correspondingly, which may suggest that Cr promotes the formation of V-based phase in the alloys. The variation of phase abundance of the C14 Laves phase and the V-based phase could affect the overall performance of the hydrogen storage alloy electrodes. Furthermore, the increasing Cr content in the alloys led to shrinkage of cell volumes of the both phases (see Fig. 2). From $x = 0$ to 0.7, the cell volume shrinkage ($\Delta V/V$) of the V-based phase is 1.48%, while the C14's is 0.17%.

Composition of the two phases determined by EDX is listed in Table 2. It can be seen that the Cr element exists mainly in the V-based solid solution. With the increasing of stoichiometry x from 0.0 to 0.7, the atomic percentage of

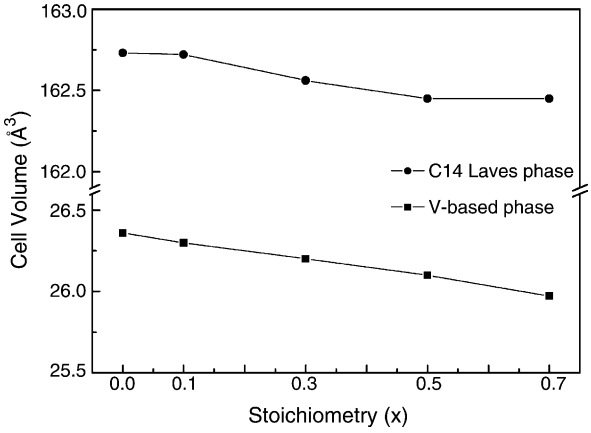

Fig. 2. Cell volume of the C14 Laves phase and V-based solid solution phase in the $Ti_{0.8}Zr_{0.2}V_{2.7}Mn_{0.5}Cr_xNi_{1.75}$ ($x = 0 \sim 0.7$) hydrogen storage alloys.

Table 1
The characteristics of phases in the $Ti_{0.8}Zr_{0.2}V_{2.7}Mn_{0.5}Cr_xNi_{1.75}$ ($x = 0.0, 0.1, 0.3, 0.5, 0.7$) alloys

Sample, x	Phase	Lattice parameter (Å)		Cell volume (Å^3)	Abundance (wt.%)
		a	c		
0.0	C14	4.868	7.930	162.73	46.2
	VSS	2.976		26.36	53.8
0.1	C14	4.869	7.925	162.72	36.1
	VSS	2.974		26.30	63.9
0.3	C14	4.868	7.922	162.56	35.1
	VSS	2.970		26.20	64.9
0.5	C14	4.865	7.924	162.45	31.3
	VSS	2.966		26.10	68.7
0.7	C14	4.868	7.917	162.45	22.2
	VSS	2.961		25.97	77.8

Table 2
The composition of phases in the $Ti_{0.8}Zr_{0.2}V_{2.7}Mn_{0.5}Cr_xNi_{1.75}$ ($x = 0.0, 0.1, 0.3, 0.5, 0.7$) alloys

Sample, x	Phase	Composition (at.%)					
		Ti	Zr	V	Mn	Cr	Ni
0.0	C14	22.13	6.67	15.34	5.67	0.00	50.19
	VSS	7.68	0.07	67.53	11.17	0.00	13.54
0.1	C14	23.38	7.63	11.43	5.34	0.12	52.09
	VSS	6.06	0.14	68.91	10.15	2.43	12.32
0.3	C14	22.63	7.44	13.32	5.74	0.47	50.39
	VSS	4.93	0.22	66.36	9.37	7.90	11.22
0.5	C14	24.19	5.97	13.87	6.02	0.74	49.20
	VSS	5.32	0.09	61.58	8.64	13.00	11.38
0.7	C14	26.10	6.81	10.72	4.66	1.09	50.62
	VSS	3.57	0.12	61.15	8.72	16.98	9.46

Cr in the V-based solid solution increased markedly from 0 to 16.98 at.%, while for the C14 phase, slightly from 0 to 1.09 at.%. This is in good accordance with the cell volume shrinkage of the two phases, which make us believe that the cell volume shrinkage is due to the relatively small radius of Cr among the six constituent elements.

Fig. 3 shows the SEM micrographs of the $Ti_{0.8}Zr_{0.2}V_{2.7}Mn_xCr_{0.8}Ni_{1.75}$ ($x = 0.0 \sim 0.7$) alloys. It can be seen that all the alloys have a dendritic V-based phase surround by continuous C14 Laves phase. With the increasing x from 0 to 0.7, the V-based phase dendrites and the C14 Laves phase both gradually grow thicker.

Fig. 4 shows the cycle life curves of the $Ti_{0.8}Zr_{0.2}V_{2.7}Mn_{0.5}Cr_xNi_{1.75}$ ($x = 0.0 \sim 0.7$) alloy electrodes. The maximum discharge capacity and cyclic stability parameters are presented in Table 3. It can be seen that the cyclic stability of the alloy electrode is improved dramatically as the stoichiometry x increases. For the sample $x = 0.0$, the discharge capacity of the electrode remains 25.4% of the maximum discharge capacity after 180 charge–discharge cycles, while for the sample $x = 0.7$ the figure is 93.8%.

Meanwhile, the maximum discharge capacity increased with increasing x from 309 mAh/g ($x = 0.0$) to 322 mAh/g ($x = 0.3$) and then decreased to 277 mAh/g ($x = 0.7$). As mentioned above, the increasing Cr content leads to cell volume shrinkage of both C14 Laves and V-based phase in the alloy, which could result in a capacity decline. Besides, Cr cannot form stable hydride, the increasing Cr content could lead to a proportion decrease of hydrogen storage elements such as Ti, Zr, V and thus reduce the capacity of the alloy electrodes.

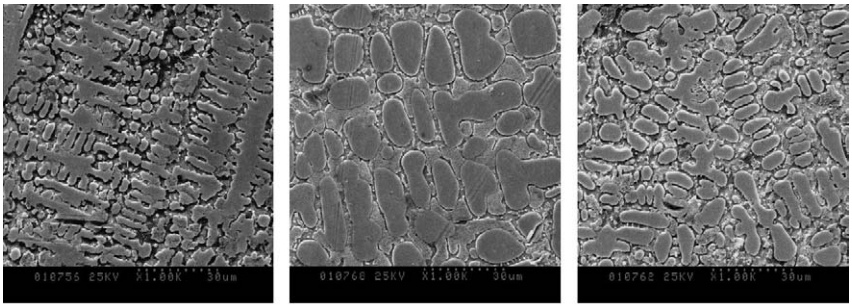

Fig. 3. SEM micrographs of the $Ti_{0.8}Zr_{0.2}V_{2.7}Mn_{0.5}Cr_xNi_{1.75}$ ($x = 0 \sim 0.7$) alloys. (a) $x = 0.0$ (b) $x = 0.3$ (c) $x = 0.7$.

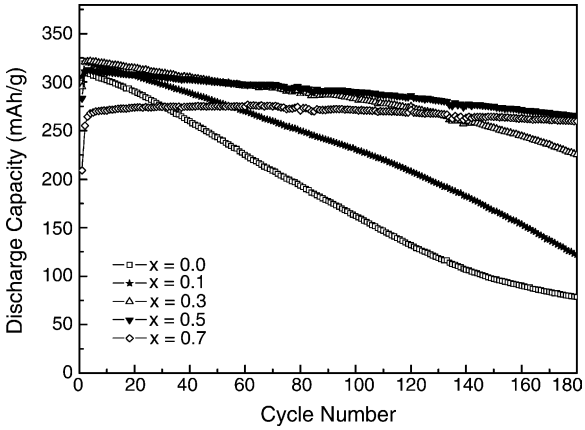

Fig. 4. Discharge capacity vs. cycle number of the $Ti_{0.8}Zr_{0.2}V_{2.7}Mn_{0.5}Cr_xNi_{1.75}$ ($x = 0 \sim 0.7$) alloy electrodes at 303 K.

But the most important factors to the TiV-based two-phase alloy's hydrogen storage capacity are the phase composition, abundance and distribution in the alloys [4,8]. It has been approved that of the two main constituent phases in Ti–V-based alloys, the V-based solid solution phase is the major hydrogen-absorbing phase while the C14 Laves phase not only absorbs hydrogen, but also works as a catalyst and micro-current collector for the V-based phase [5]. Appropriate proportion of the two phases and fine equiaxed microstructures are favorable for C14 phase to take the catalyzing and micro-current collecting effect; while insufficient C14 Laves phase and thick dendrite microstructures may debase the catalyzing effect and thus diminish the capacity [4]. In this work, the Rietveld analysis showed that the abundance of the V-based solid solution phase increased rapidly from 53.8 to 63.9 wt.% when the stoichiometry of Cr increased from 0 to 0.1, since the V-based solid solution phase is the major hydrogen-absorbing phase, the rapid increase of it may counteracted the disadvantages mentioned above and lead to a slight increase of capacity. But along with the further increase of Cr content, the proportion of the two phases became undesirable and the V-based phase dendrites and the C14 Laves phase both gradually grew thicker. All these disadvantages resulted in the decline of the capacity from 322.0 mAh/g ($x = 0.3$) to 276.6 mAh/g ($x = 0.7$).

Fig. 5 shows the high rate dischargeability (HRD) of the $Ti_{0.8}Zr_{0.2}V_{2.7}Mn_{0.5}Cr_xNi_{1.75}$ ($x = 0.0 \sim 0.7$) alloy electrodes. With the increasing Cr content, the HRD of the alloy electrode improved at first and then declined. At the discharge current of 600 mAh/g, the HRD of the alloy electrodes increased from 27.5% ($x = 0.0$) to 71.2% ($x = 0.5$) and then decreased to 54.7% ($x = 0.7$). According to the electrochemical theory, the process of discharging of hydrogen storage alloy electrodes includes three steps: (1) absorbed hydrogen diffuse from the interior to the surface of the alloy particles; (2) absorbed hydrogen transform into adsorbed hydrogen at the surface of the alloy particles; (3) adsorb hydrogen take charge transfer reactions at the surface of the alloy particles. Therefore, the HRD is believed to be mainly controlled with both the charge transfer resistance at the electrode surface and the hydrogen diffusion resistance inside the electrode. To further the investigation of the kinetics of the alloy electrodes, a series of electrochemical methods, namely the electrochemical impedance spectroscopy (EIS), the linear polarization, the anode polarization and the potentiostatic discharge have been employed.

Table 3
Capacity and cyclic stability of the $Ti_{0.8}Zr_{0.2}V_{2.7}Mn_{0.5}Cr_xNi_{1.75}$ ($x = 0.0$, 0.1, 0.3, 0.5, 0.7) alloy electrodes

Sample, x	C_{max} (mAh/g)	C_{100}/C_{max} (%)	C_{180}/C_{max} (%)
0.0	309	52.4	25.4
0.1	321	71.9	38.0
0.3	322	87.8	70.0
0.5	313	92.8	84.9
0.7	277	98.1	93.8

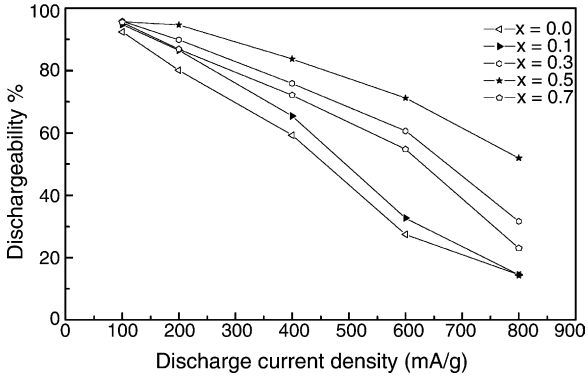

Fig. 5. HRD of the $Ti_{0.8}Zr_{0.2}V_{2.7}Mn_{0.5}Cr_xNi_{1.75}$ ($x = 0 \sim 0.7$) alloys electrodes at 303 K.

Fig. 6 shows the EIS of the $Ti_{0.8}Zr_{0.2}V_{2.7}Mn_{0.5}Cr_xNi_{1.75}$ ($x = 0.0 \sim 0.7$) alloy electrodes at 50% DOD. It can be found that all the EIS curves consist of two semicircles followed with a straight. According to the analysis model proposed by Kuriyama et al. [13], the semicircle in the high-frequency

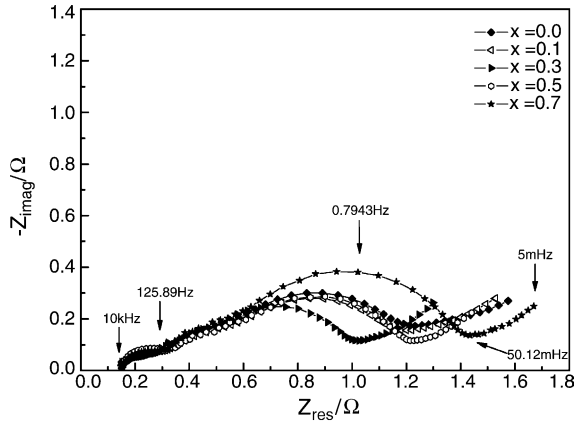

Fig. 6. Electrochemical impedance spectroscopy of the $Ti_{0.8}Zr_{0.2}V_{2.7}Mn_{0.5}Cr_xNi_{1.75}$ ($x = 0 \sim 0.7$) alloy electrodes measured at the 50% DOD and 298 K.

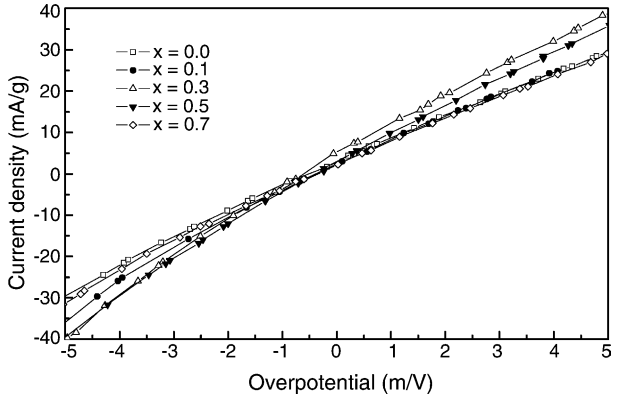

Fig. 7. Linear polarization curves for the $Ti_{0.8}Zr_{0.2}V_{2.7}Mn_{0.5}Cr_xNi_{1.75}$ ($x = 0 \sim 0.7$) alloy electrodes with a scan rate of 0.1 mV/s measured at the 50% DOD and 298 K.

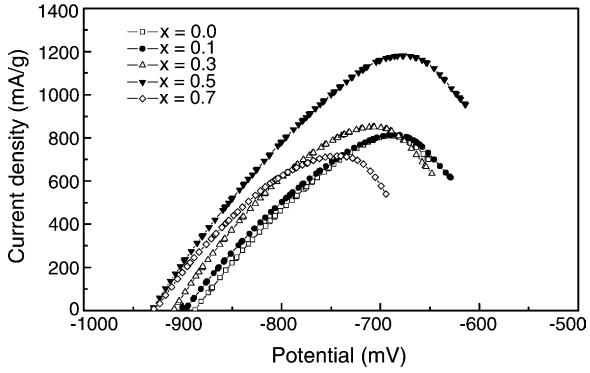

Fig. 8. Anode polarization curves for the $Ti_{0.8}Zr_{0.2}V_{2.7}Mn_{0.5}Cr_xNi_{1.75}$ ($x = 0 \sim 0.7$) alloy electrodes with a scan rate of 5 mV/s measured at 50% DOD and 298 K.

region is mainly related to the resistance and capacitance between the alloy particles and the current collector, while the semicircle in the low-frequency region is attributed to the charge transfer resistance for hydrogenation reaction at the surface. From the variation of the radius of the semicircle in the low-frequency region, it can be estimated that the charge transfer resistance of the alloy electrodes decreased first and then increased with increasing Cr content.

Fig. 7 shows the linear polarization plots of the $Ti_{0.8}Zr_{0.2}V_{2.7}Mn_{0.5}Cr_xNi_{1.75}$ ($x = 0.0 \sim 0.7$) alloy electrodes. It can be seen from the variation of slopes of the plots that the reaction resistance of the electrodes decreased first and then increased with increasing x, identically with the conclusion out of the EIS. The exchange current density I_0 was calculated by the following formula [14] and listed in Table 4.

$$I_0 = \frac{IRT}{F\eta} \tag{1}$$

R, T, F and η denote the gas constant, the absolute temperature, the Faraday constant and the overpotential, respectively. I_0 increased from 139 mA/g ($x = 0.0$) to 181 mA/g ($x = 0.3$) and then decreased to 138 mA/g ($x = 0.7$).

Fig. 8 shows the anode polarization curves of the $Ti_{0.8}Zr_{0.2}V_{2.7}Mn_{0.5}Cr_xNi_{1.75}$ ($x = 0.0 \sim 0.7$) alloy electrodes. The limiting current densities I_L obtained from the figure are listed in Table 4. It can be seen that the limiting current density I_L increased from 809 mA/g ($x = 0.0$) to 1182 mA/g ($x = 0.5$) and then decreased to 717 mA/g ($x = 0.7$), which is consistent with the variation of the HRD of the alloy electrodes.

Fig. 9 shows the plots of potentiostatic discharge, namely the discharge current decay with the time of the $Ti_{0.8}Zr_{0.2}V_{2.7}Mn_{0.5}Cr_xNi_{1.75}$ ($x = 0.0 \sim 0.7$) alloy electrodes. It can be seen that under the operation of the potential step, the current–time responses in the semilogarithmic plot ($\log i$ versus t) can be divided into two time regions as proposed by Nishina et al. [15]. In the first region, the current declines abruptly due to the fast consumption of hydrogen on the surface of the alloy particles. In the second region, the current declines relatively slowly in a linear manner. In this case, the current was mainly controlled by the hydrogen diffusion velocity, which is proportional to the concentration gradient of hydrogen in the bulk of the alloy. Therefore the linear response in the second region can be treated as the finite diffusion of hydrogen atoms inside the alloy particle according to the spherical diffusion model [15]. The hydrogen diffusion coefficient D can be estimated by the following formulas [16] and listed in Table 4:

$$\log i = \log\left[\pm\frac{6FD}{\mathrm{d}a^2}(C_0 - C_S)\right] - \frac{\pi^2}{2.303}\frac{D}{a^2}t \tag{2}$$

where i denotes the diffusion current density (A/g), D the hydrogen diffusion coefficient (cm^2/s), C_0 the initial hydrogen concentration (mol/cm^3) inside the alloy particles, C_S the hydrogen concentration (mol/cm^3) at the surface of the alloy particles, a denotes the radius of alloy particles (cm), d denotes the density of the hydrogen storage alloy (g/cm^3) and t denotes the discharge time (s). It can be found that, consistently to the variation of the limiting current density I_L, the diffusion coefficient D increased from 2.82×10^{-11} cm^2/s ($x = 0.0$) to 7.32×10^{-11} cm^2/s ($x = 0.5$) and then decreased to 4.75×10^{-11} cm^2/s ($x = 0.7$).

The kinetic properties in the hydride electrode are generally controlled with both the charge transfer resistance at surface of the alloy particles and the hydrogen diffusion resistance inside the alloy particles. In other words, the HRD is influenced jointly by the exchange current density I_0, the

Table 4
The exchange current density I_0, limiting current density I_L and hydrogen diffusion coefficient D of the $Ti_{0.8}Zr_{0.2}V_{2.7}Mn_{0.5}Cr_xNi_{1.75}$ ($x = 0.0 \sim 0.7$) alloy electrodes

Sample, x	I_0 (mA/g)	I_L(mA/g)	$D \times 10^{11}$ (cm^2/s)
0.0	139	809	2.82
0.1	172	815	4.14
0.3	181	851	6.01
0.5	170	1182	7.32
0.7	138	717	4.75

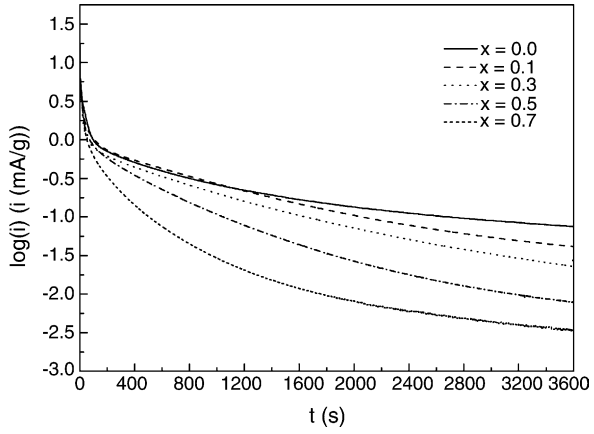

Fig. 9. Semilogarithmic plots of anodic current vs. time responses of the $Ti_{0.8}Zr_{0.2}V_{2.7}Mn_{0.5}Cr_xNi_{1.75}$ ($x = 0 \sim 0.7$) alloy electrodes.

limiting current density I_L and the hydrogen diffusion coefficient D. In this work, I_0, I_L and D all increased first and then decreased with the increasing Cr content in the alloys. But the corresponding compositions of the maximums are somewhat different, for I_0 it's $x = 0.3$; for I_L and D it's $x = 0.5$, identical with the high rate dischargeability. Considering that I_0 reflects the charge transfer resistance while I_L and D reflect the diffusion resistances, it can be inferred that HRD of the $Ti_{0.8}Zr_{0.2}V_{2.7}Mn_{0.5}Cr_xNi_{1.75}$ ($x = 0.0 \sim 0.7$) alloy electrodes are controlled with both the charge transfer resistance and the hydrogen diffusion resistances, but mainly the latter.

4. Conclusions

Phase structures and electrochemical properties of the $Ti_{0.8}Zr_{0.2}V_{2.7}Mn_{0.5}Cr_xNi_{1.75}$ ($x = 0 \sim 0.7$) alloys were systematically investigated to get an overall evaluation of Cr in the TiV-based alloys. It was found by XRD and Rietveld analysis that all the alloys consisted of a C14 Laves phase and a V-based solid solution phase. With the increasing Cr contents, the abundance, distribution, composition and lattice parameters of the V-based phase and the C14 Laves phase varied markedly and affected the synergism of the two phases. Besides the anticipated improvement of cyclic life, the increasing Cr content also lead to a better high rate dischargeability (HRD) in a certain range, but the discharge capacity may decrease with excessive Cr. Electrochemical impedance spectroscopy (EIS), linear polarization, anode polarization and potentiostatic discharge tests indicated that HRD of the alloy electrodes were mainly controlled with hydrogen diffusion resistances.

Acknowledgment

This work was supported by National Natural Foundation of China under contract No. 50271063.

References

[1] H.G. Pan, Y.F. Zhu, M.X. Gao, Y.F. Liu, R. Li, Y.Q. Lei, Q.D. Wang, Q.D. Wang, J. Alloys Compd. 364 (2004) 271.
[2] Y.F. Zhu, H.G. Pan, M.X. Gao, Y.F. Liu, Q.D. Wang, J. Alloys Compd. 347 (2002) 279.
[3] Y.F. Zhu, H.G. Pan, M.X. Gao, Y.F. Liu, Q.D. Wang, J. Alloys Compd. 348 (2003) 301.
[4] R. Li, H.G. Pan, M.X. Gao, Y.F. Zhu, Y.F. Liu, Q.W. Jin, Y.Q. Lei, J. Alloys Compd. 373 (2004) 223.
[5] H.G. Pan, Y.F. Zhu, M.X. Gao, Y.F. Liu, R. Li, Y.Q. Lei, Q.D. Wang, J. Alloys Compd. 370 (2004) 254.
[6] Y.F. Zhu, H.G. Pan, G.Y. Wang, M.X. Gao, J.X. Ma, C.P. Chen, Q.D. Wang, Int. J. Hydrogen Energy 26 (2001) 807.
[7] Y.F. Zhu, H.G. Pan, M.X. Gao, J.X. Ma, S.Q. Li, Q.D. Wang, Int. J. Hydrogen Energy 27 (2002) 287.
[8] H.G. Pan, Y.F. Zhu, M.X. Gao, Q.D. Wang, J. Electrochem. Soc. 149 (2002) 829.
[9] J.S. Yu, S.M. Lee, K. Cho, J.Y. Lee, J. Electrochem. Soc. 147 (2000) 2013.
[10] H.H. Lee, K.Y. Lee, J.Y. Lee, J. Alloys Compd. 260 (1997) 201.
[11] J.H. Kim, H.L. Lee, P.S. Lee, C.Y. S, J.Y. Lee, J. Alloys Compd. 348 (2003) 293.
[12] F. Izumi, R.A. Young (Eds.), The Rietveld Method, Chapter 13, Oxford University Press, Oxford, 1993.
[13] N. Kuriyama, T. Sakai, H. Miyamura, I. Uehara, H. Ishikawa, J. Alloys Compd. 202 (1995) 183.
[14] P.H.L. Notten, P. Hokkeling, J. Electrochem. Soc. 138 (1991) 1877.
[15] T. Nishina, H. Ura, I. Uchida, J. Electrochem. Soc. 144 (1997) 1273.
[16] G. Zhang, B.N. Popov, R.E. White, J. Electrochem. Soc. 142 (1995) 2695.